SUPPLEMENTARY APPENDIX

Cytoskeletal-based mechanisms differently regulate *in vivo* and *in vitro* proplatelet formation

Alicia Bornert,[1] Julie Boscher,[1] Fabien Pertuy,[1] Anita Eckly,[1] David Stegner,[2] Catherine Strassel,[1] Christian Gachet,[1] François Lanza[1] and Catherine Léon[1]

[1]Université de Strasbourg, INSERM, EFS Grand-Est, BPPS UMR-S 1255, Strasbourg, France and [2]Institute of Experimental Biomedicine, University Hospital Würzburg & Rudolf Virchow Center for Experimental Biomedicine, University of Würzburg, Würzburg, Germany

 doi:10.3324/haematol.2019.239111

Received: September 23, 2019.

Accepted: April 14, 2020.

Pre-published: April 23, 2020.

Correspondence: *CATHERINE LÉON* - catherine.leon@efs.sante.fr

Supplemental Data

Cytoskeletal-based mechanisms differently regulate *in vivo* and *in vitro* proplatelet formation

Alicia Bornert[1], Julie Boscher[1], Fabien Pertuy[1], Anita Eckly[1], David Stegner[2], Catherine Strassel[1], Christian Gachet[1], François Lanza[1], Catherine Léon[1*]

Supplemental Materials and Methods.

Materials

Vascular Labels Qtracker™ 655, DAPI and ProLong Gold were purchased from Invitrogen (Eugene, OR, USA). Vincristine and bovine serum albumin (BSA) were from Sigma-Aldrich (Rueil-Malmaison, France). The Alexa Fluor 488-labeled anti-GPIX antibody derivatives were kindly provided by Prof. Dr. Bernhard Nieswandt (Institute of Experimental Biomedicine, University Hospital Würzburg, Germany)[52]. The anti-GPIbβ antibody (RAM1) was produced in our laboratory and the AF488-labeled anti-α tubulin antibody was from Invitrogen (clone DM1A). Histoacryl surgical glue was from Braun Surgical (Rubí, Spain). Dental paste (Picodent twinsil speed) was from Picodent (Wipperfürth, Germany).

Mice

Male and female mice between 5 and 7 weeks old were used for intravital imaging. *mT/mG;Pf4-cre* mice were generated by crossing B6.129(Cg)-*Gt(ROSA)26Sor*$^{tm4(ACTB-tdTomato,-EGFP)Luo}$/J with *Pf4-cre* mice to obtain eGFP expression in MKs and platelets, as described previously[53]. Mice deficient in myosin IIA (*Myh9*$^{-/-}$ mice)[54], mice lacking β1 tubulin (*Tubb1*$^{-/-}$ mice)[28] and control mice had a C57BL/6J genetic background. Animal experiments were performed in accordance with European law and the recommendations of the Review Board of the Etablissement Français du Sang (EFS) and the Institut de

Génétique et de Biologie Moléculaire et Cellulaire (IGBMC) regarding animal care and agreement for experimentation obtained from the French government.

Intravital imaging

Mice were anesthetized by injection of a solution of ketamine (100 µg/g) and xylazine (10 µg/g). The scalp was incised at the midline to expose the calvarium and the periosteum was removed without damaging the bone. A 3D printed ring was glued to the mouse skull using surgical glue and silicone dental paste was deposited around the ring to prevent leakage. The ring was filled with physiological saline to keep the skull wet and serve as an immersion medium for the microscope objective. The mouse was placed on a temperature-controlled plate at 37°C during surgery and kept for a maximum of 3h under the microscope inside an environmental chamber at 37°C, in agreement with the local ethical and animal welfare comity. Although the visualized events are relatively rare, this time was sufficient to record elongation from already extended nPPTs. The anesthesia was re-induced every 35 min by alternating subcutaneous injections of ketamine (25 µg/g) and a mixture of ketamine (50 µg/g) and xylazine (5 µg/g). To characterize PPTs, we used *mT/mG;Pf4-cre* whose MKs express the fluorescent reporter protein. To evaluate nPPT formation in knockout animals, MKs and platelets were stained by intravenous injection of an AF488-conjugated anti-GPIX antibody derivative[52]. Of note, nPPTs exhibited identical morphologies whether they were observed from mT/mG;Pf4-cre mice or mice injected with the antibody (Suppl. Fig. S1C shows the measured nPPT width for both mouse models). The BM vasculature was visualized by intravenous injection of Qtracker 655. In some mice, vincristine (100 µL) was administered at a dose of 1 or 2 mg/kg to give respectively a final concentration of about 10 or 20 µg/mL (≈ 10 or 20 µM) in the circulating blood, assuming a total blood volume of 2 mL/mouse.

Two-photon microscopy

Intravital imaging was performed using a Leica SP8 confocal microscope equipped with a 25x water objective with a numerical aperture of 0.95 (Leica) (IGBMC/CBI plateform, Illkirch) or a Leica MP

DIVE (EFS, Strasbourg). A femtosecond Ti:Saph pulsing laser (Coherent) was used at 913 nm to simultaneously excite AlexaFluor-488 and Qtracker-655. The emitted light was detected using non-descanned HyD hybrid detectors with 525/25 and 617/73 filters. Images were recorded with a resonant scanner (12 kHz for the SP8, 8 kHz for the MP DIVE) in bidirectional mode and an adapted averaging.

Acquisition and analysis of nPPT images

To study PPT formation, the x-y surface area (384 x 384 pixels) was visualized at 10 s intervals and z-stack images were acquired with z-depths of 1.34 µm. All images were analyzed with ImageJ software (National Institute of Health, Bethesda, MD). The profiles were aligned if necessary using the ImageJ template matching plug-in and an average z-projection was obtained. Depending on the image quality, the background was subtracted, the image was smoothed and the brightness and contrast adjusted. To measure the width of nPPT, a perpendicular line was drawn at a fixed position close to the base of the nPPT and the profile intensity was recorded at this position every minute (see Suppl. Fig. S1A). A Gaussian curve was fitted to this profile and the FWHM (Full Width at Half Maximum) was considered to represent the width of the nPPT. The mean width was then calculated by averaging the widths of the nPPT measured at each time point at the fixed position. The maximal nPPT length was also determined, from the base of the nPPT to its tip. The net mean nPPT elongation speed (including pause and retraction) was calculated as the change in nPPT length at one minute intervals and averaged over the whole time sequence. To better highlight the pauses and retractions upon the process of nPPT growth, the length measured every 10 sec was represented as a percentage of the maximal length of each individual nPPT, mentioned in the Figure legend. For the vincristine experiments, the length and width measurements were done once immediately before drug administration and other measurements were performed every minutes, from 0.5 min after vincristine injection to up to 15 min for some PPTs. Measurements of cPPTs were performed on phase contrast imaged from cPPT extended in the explant model. The same method as above was used, except for the bud width where a threshold was applied before measurements.

Measurement of Blood flow

Blood flow was estimated by measuring the displacement of circulating platelets within a small x-y area (256 x 90 pixels) to maximize the frame acquisition rate. A maximum of 133 frames/s could be obtained and displacement were usually acquired during 20 seconds. The blood flow in a portion of a vessel was determined using ImageJ line-scan software at three different positions, i.e. in the center and close to opposite vessel walls. The resulting images represent the successive linear scans stacked over time. These space-time images shows the moving platelets, as diagonal streaks, where the slope is related to their velocity. The images were then exported into GNU Octave software to determine the flow velocity using the Radon transform method[55].

***In vitro* proplatelet formation.**

For explant bone marrow experiments, marrows were flushed out of mouse femurs and cut into transverse sections of 0.5 mm-thick. Megakaryocytes were observed after 6 h of incubation at 37°C, at the periphery of the tissue, as described[26].

In vitro liquid culture of Lin^- mouse progenitors was performed as described previously[56]. Bone marrow cells were flushed from femurs and tibias from 8- to 12-week old male C57Bl/6 mice and successively passed through 21-, 23- and 25-gauge needles. The cells were spun down and nucleated cells were counted. Cells were pelleted at 300g for 7 min and resuspended at 1×10^8 cells/ml in PBS supplemented with 2% (v/v) FBS and 2 mM EDTA to perform the lineage (Lin) negative selection, according to the recommendations of the manufacturer (Stem Cell Technologies). The Lin^- population was adjusted to 2×10^6 cells/mL in DMEM containing 2 mM glutamine, penicillin/streptomycin, 10% FBS, 50 ng/mL TPO and 100 U/mL hirudin (complete medium). Cultures were performed in 24-well tissue culture plates using 500 µL of cell suspension in liquid medium per well and were incubated at 37 °C under a 5% CO_2 atmosphere. MKs extended PPTs after 4 days culture.

Immunofluorescence and confocal observations

For *in situ* immunolabeling of bone marrow, we took care to preserve the cytoskeleton. For that, we first injected 200 µL/20g mouse of a 5 mM Paclitaxel solution intravenously (i.v.) into anesthetized mice. After 3 min a second i.v. injection of 300 µL PFA 12% was performed, femurs were immediately removed and the marrow was flushed directly into the fixative solution (4% PFA in PHEM buffer containing 50 µM Paclitaxel and 100 nM phalloidin). After fixation for 24 h and cryopreservation in sucrose, the marrow was embedded in freezing medium and cryosections 30 µm were cut. Immunolabeling on thick marrow sections was performed by O/N incubation with AF-488 labeled anti-α tubulin antibody (10 µg/mL), 1-h washes and incubation with AF-555 labeled anti-GPIbβ antibody (10 µg/mL) for 1 more hour, then mounting in ProLong Gold.

For platelet labeling, blood was drawn from the abdominal aorta of anesthetized mice and 0.38% citrated platelet rich plasma (cPRP) was prepared by blood centrifugation (10 min, 250g), then fixed in 4% PFA and cytospun. For cPPT labeling, 4-days cultured MKs were fixed in 4% PFA and cytospun. Immunolabeling was done using the same antibodies and protocol as described above for *in situ*, except for anti-tubulin antibody which was incubated only for 1 h.

Images were acquired using a Leica SP8 inverted confocal microscope, equipped with a 63x oil immersion objective (1.4 NA) and Leica Application Suite software (LASX). Images are either a single z-plane, or a z-stack and 3D reconstruction (Fig. 1Ai-ii and 4C). The presented images are the raw images without any post-treatment except for Fig. 4B and C where a deconvolution treatment was applied using Huygens software. The proportion of PPT fragments from WT and *Tubb1*$^{-/-}$ was quantified by performing z-stack acquisitions (dimension of the acquisition field 400 x 400 x 30 µm). A 3D reconstruction using LASX and observations in all directions allowed to visualized MKs and PPT fragments. We considered a PPT fragment any GPIbβ-positive element having a rod-like shape longer than 15 µm.

Scanning electron microscopy.

To visualize the intracellular cytoskeletal filaments, cultured megakaryocytes were incubated for 5 min with 0.5% Triton X-100 in PHEM containing 0.1% glutaraldehyde, 5 μM phalloidin and 30 μM taxol. The resulting cytoskeletons were fixed in 1% glutaraldehyde for 10 min and allowed to adhere by sedimentation to the surface of poly-L-lysine-coated coverslips. After three washes in PBS and dehydration in graded ethanol solutions, the samples were air-dried with hexamethyldisilazane, sputtered with gold and examined under a scanning electron microscope (Sirion, FEI, The Netherlands). For cPPT, samples were fixed with 2.5% glutaraldehyde in 0.1 M cacodylate buffer (pH 7.2) and prepared for SEM observation as above, without the detergent step. For the *in situ* marrow nPPT visualization, the dehydrated whole marrow fragment was further fragmented.

Statistics.

Data are presented as mean ± standard error of mean (sem). Comparison between 2 groups were performed using two-tailed Student's t-test or Mann-Whitney test when number was too small or when the population did not pass the normality test, mentioned in figure legends.*, $p<0.05$; **, $p<0.01$; ***, $p<0.0001$; ns, $p>0.05$

Legends to Supplemental Figures and videos

Supplemental Figure S1. Morphological characteristics of *in vivo* PPTs. A) Upper, z-projection image depicting the site where the nPPT width was measured together with maximal length. Middle, maximal length of 25 individual nPPTs obtained from 14 mice. The same color has been attributed to nPPT observed in the same mouse. Bottom, mean nPPT width measured at the base of the nPPT over the course of elongation for 28 individual nPPTs obtained from 19 mice. Bars are mean±sem of the width measured every minutes during acquisition. The same color has been attributed to nPPT observed in the same mouse. B) Time lapse showing nPPT detaching from its base. C) Mean nPPT width showing no difference between mTmG/Pf4-cre mice (15 nPPTs pooled from 10 mice) and WT mice injected with the anti-GPIX antibody (13 nPPTs pooled from 9 mice) (ns, not significant with unpaired Student't t-test).

Supplemental Figure S2. Presence of pauses and retractions in WT mice while absence in *Myh9*$^{-/-}$ mice. A) Scatter plot representing the nPPT elongation speed calculated in WT mice. Individual values and mean ± sem. Data are 12 nPPTs pooled from 8 mice. B-C) Individual tracings showing the elongation behavior of WT (B) and *Myh9*$^{-/-}$ (C) nPPT, some of the WT nPPT presenting pause and retraction phases while they are absent during the course of *Myh9*$^{-/-}$ nPPT elongation. Data presented as the % of maximal nPPT length. Data are 11 nPPTs pooled from 10 WT mice and 6 nPPTs pooled from 4 *Myh9*$^{-/-}$ mice.

Supplemental Figure S3. Decreased PPT fragments and platelet count in *Tubb1-/-* mice but normal granule distribution. A) 3D view rendering of 30 µm-thick WT or *Tubb1*$^{-/-}$ marrow sections

acquired by confocal microscopy, immunolabeled for GPIbβ to visualize MKs and platelets (magenta). Arrows show nPPTs or nPPT fragments longer than 15 µm. Note the higher number of MKs in the *Tubb1*$^{-/-}$ marrow. B) Left, quantification of platelet counts in circulating blood of 18-days or 8-weeks old WT *vs*. *Tubb1*$^{-/-}$ mice. Right, Mean platelet volume for the same mice. ***, p<0.0001 using two-tailed unpaired Student's t-test. n=6 mice. C) TEM images showing platelet ultrastructure from WT and *Tubb1-/-* mice. Representative of 2 independent platelet preparations.

Supplemental Figure S4. Impact of vincristine on WT and *Myh9*$^{-/-}$ *platelet* marginal band, *in vitro* and *in vivo*. A) Vincristine (20 µM) was added to fresh WT or *Myh9*$^{-/-}$ cPRP for the indicated time. PRP was PFA-fixed and cytospun before immunolabeling with anti-α tubulin antibody. Images are representative of 2 experiments and were acquired by confocal microscopy. Bar is 30 µm. B) Vincristing (2 mg/kg) was administered i.v. in WT or *Myh9-/-* mice for the indicated time and blood was drawn using citrate 0.38% final concentration as an anticoagulant. cPRP was prepared and fixed within less than 1.5 minutes from blood drawing. Microtubules are visualized by immunolabeling with anti-α tubulin antibody. Images representative of 3 independent experiments.

Supplemental Figure S5. *In situ* observation of microtubules and F-actin following vincristine administration.

Confocal plane images showing MK from untreated mice (left images) or from mouse injected with vincristine (1 mg/kg) (right images) for 10 minutes. A) WT mice, and B) *Myh9*$^{-/-}$ mice, top panels are GPIbα labelings, middle panels are α-tubulin labelings, and bottom panels are F-actin labelings (phalloidin). Representative of at least 3 sections from 2 mouse marrows.

Supplemental Figure S6. Impact of vincristine 1mg/kg injection on native PPT length. A) Measurement of nPPT length in *Myh9*$^{-/-}$ mice before and after 1 mg/kg vincristine administration plotted as a function of time. Seven *Myh9*$^{-/-}$ mice analyzed. B) Measurement of the difference in nPPT length

during a 10-min window post-vincristine administration (1 mg/kg), showing decreasing length in WT (n=7) (left) while increasing length despite vincristine injection in *Myh9*$^{-/-}$ mouse nPPT (n=4) (right).

Supplemental Figure S7. *In situ* observation of nPPT from *Myh9*$^{-/-}$ marrow.

Confocal image showing microtubules (AF-488 α-tubulin labeling) and F-actin (AF-647 phalloidin labeling) in a *Myh9*$^{-/-}$ PPT, visualized by anti-GPIbα labeling. Image to be compared to the WT one in Fig. 4D and E.

Supplemental Figure S8. *Myh9*$^{-/-}$ nPPT are poorly enriched in DMS. TEM images showing nPPT observed in *in situ* bone marrow sinusoids from either WT or *Myh9*$^{-/-}$ mice. Red arrows denote nPPT fragments. s, sinusoid; e, erythrocyte. Observations from 2 WT and 2 *Myh9*$^{-/-}$ mice.

Video 1: Representative time lapse video (z-projection) recording WT mouse with MK extending an elongating nPPT (green) within bone marrow sinusoids (red, Qtracker).

Video 2: Representative time lapse video (z-projection) recording WT mouse, showing a MK extending a short and large nPPT (arrow) and another MK extending a long, thin, regular and rapidly growing nPPT in the right vessel. nPPTs (green) within BM sinusoids (red, Qtracker).

Video 3: Representative time lapse video (z-projection) recording WT mouse with MK extending a very long nPPT. nPPT (green) within BM sinusoids (red, Qtracker) is shown.

Video 4: Effect of vincristine on WT PPT *in vivo*. Time lapse video recording an nPPT in WT mouse before and after administration of vincristine (1 mg/kg) (z-projection). The elongating nPPT (green) within the sinusoid vessels (red) starts to retract after intravenous administration of vincristine.

Video 5: Effect of vincristine on *Myh9*$^{-/-}$ PPT *in vivo*. Time lapse video recording of MK protrusion in *Myh9*$^{-/-}$ mouse before and after administration of vincristine (1 mg/kg) (z-projection). The elongating nPPT (green) within the sinusoid vessels (red) continue to elongate despite vincristine administration.

Video 6: Impact of mouse cardiac arrest in PPT morphology. Time lapse video recording ofn in a *Myh9*$^{-/-}$ mouse before and after cardiac arrest. The video shows 3 nPPTs (green, labeled with AF-488 anti-GPIX antibody derivative) in the same flow line before cardiac arrest, thus not individualized at the resolution of the two-photon microscopy. Following cardiac arrest, the 3 nPPTs separate and become relaxed in the absence of blood flow, but without retracting.

Video 7: Reverse flow within sinusoid. Circulating platelets (green) within the sinusoid vessels (red, Qtracker) (single confocal z-plane). An anastomosed sinusoid vessel is shown presenting bifurcations where the flow is unstable and displays phases of stasis, accelerations and decelerations.

Video 8. nPPT tossed by the reverse flows. Time lapse video showing a WT MK in the sinusoid bifurcation shown in video 4, in the process of extending an nPPT that oscillate in one vessel branch depending on the direction of flow (z-projection).

Supplemental Figure S1. Morphological characteristic of *in vivo* nPPTs

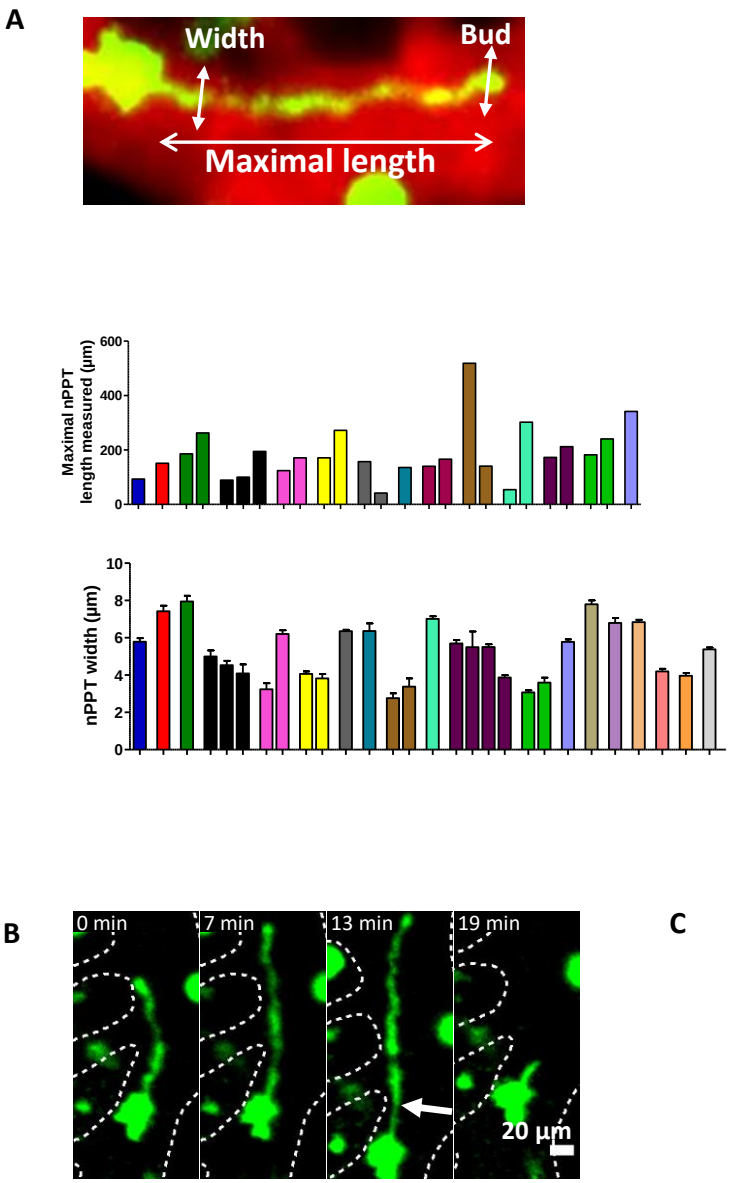

Supplemental Figure S2. Presence of pauses and retractions in WT mice while absence in *Myh9*$^{-/-}$ mice.

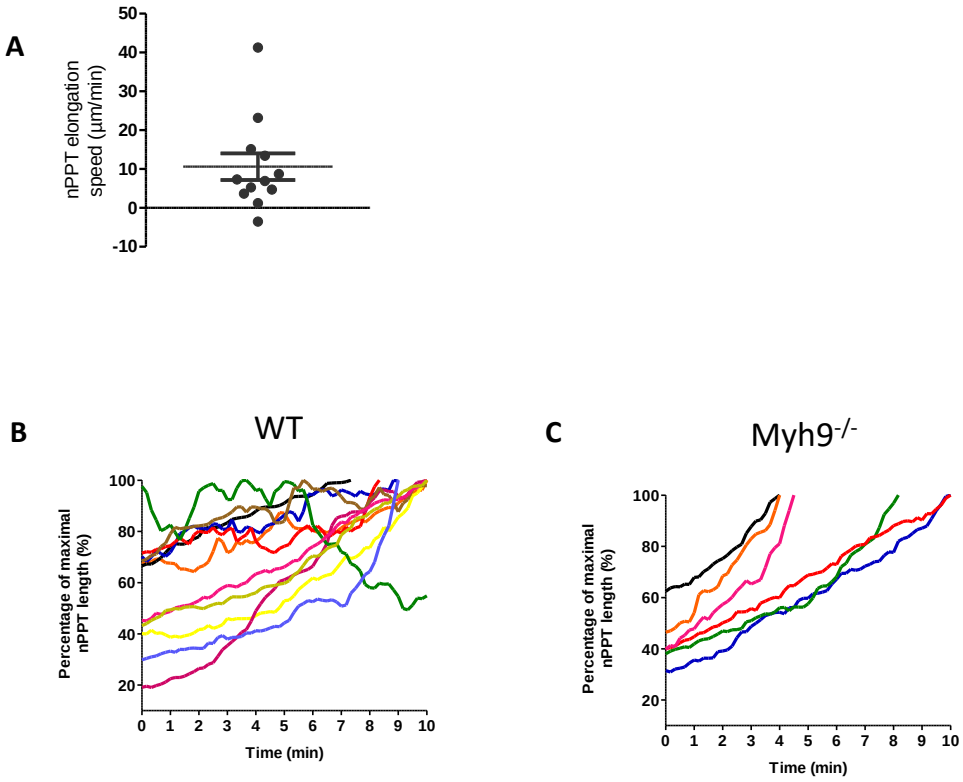

Supplemental Figure S3. Decreased nPPT fragments and platelet count in Tubb1-/- mice but normal granule distribution.

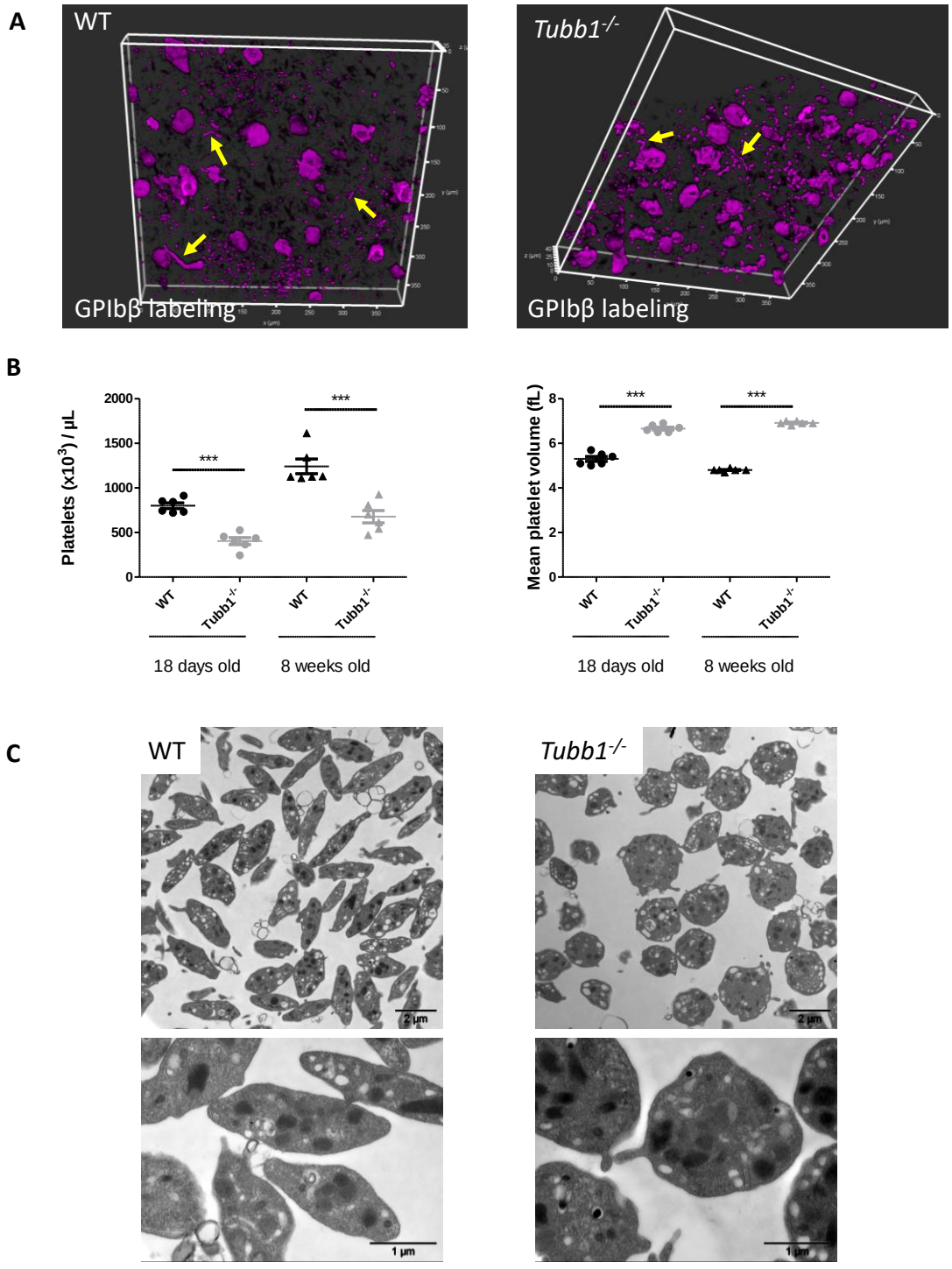

Supplemental Figure S4. Impact of vincristine on WT and *Myh9*$^{-/-}$ platelet marginal band, *in vitro* and *in vivo*

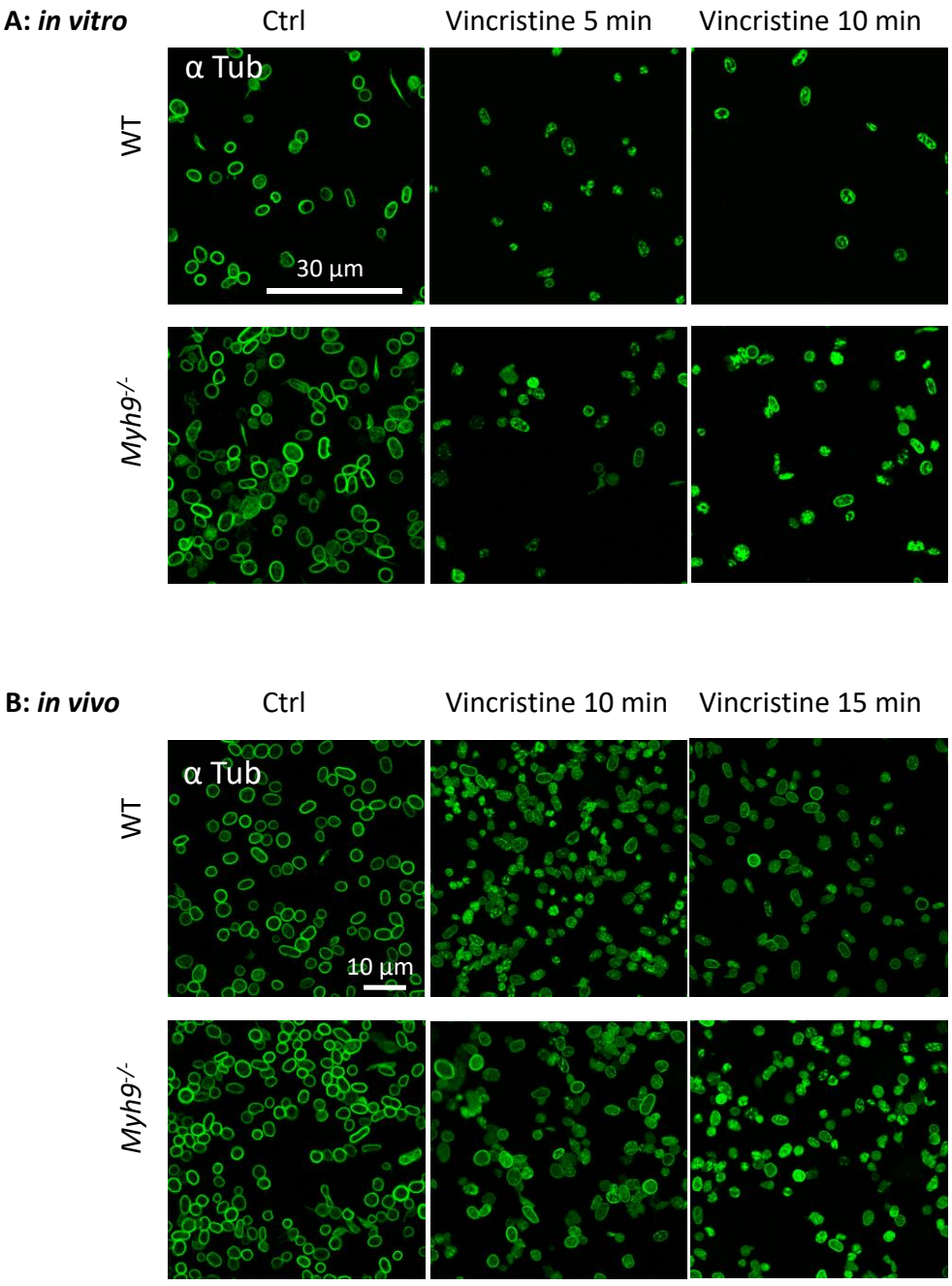

Supplemental Figure S5. *In situ* observation of microtubules and F-actin following vincristine administration.

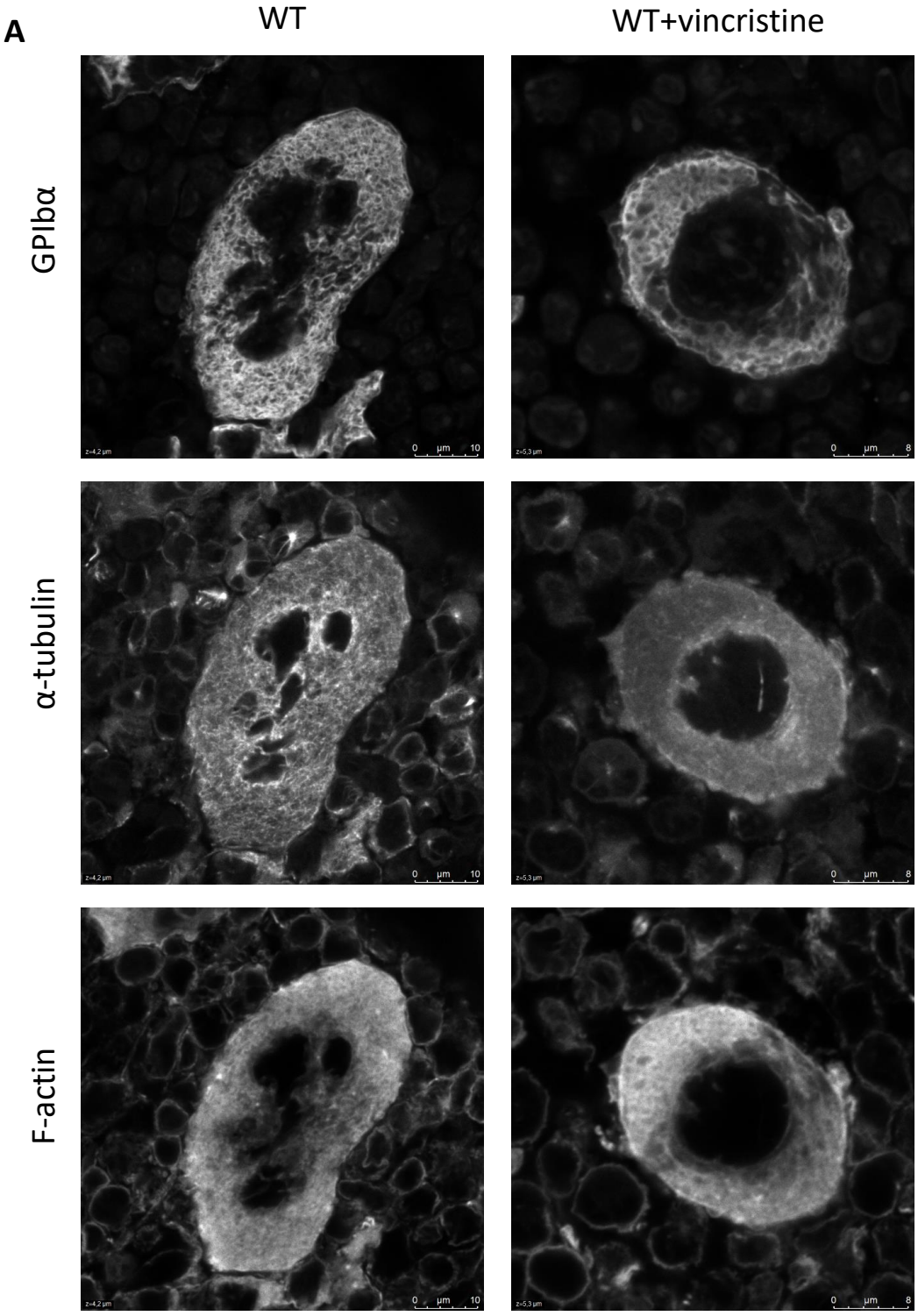

Supplemental Figure S5. *In situ* observation of microtubules and F-actin following vincristine administration.

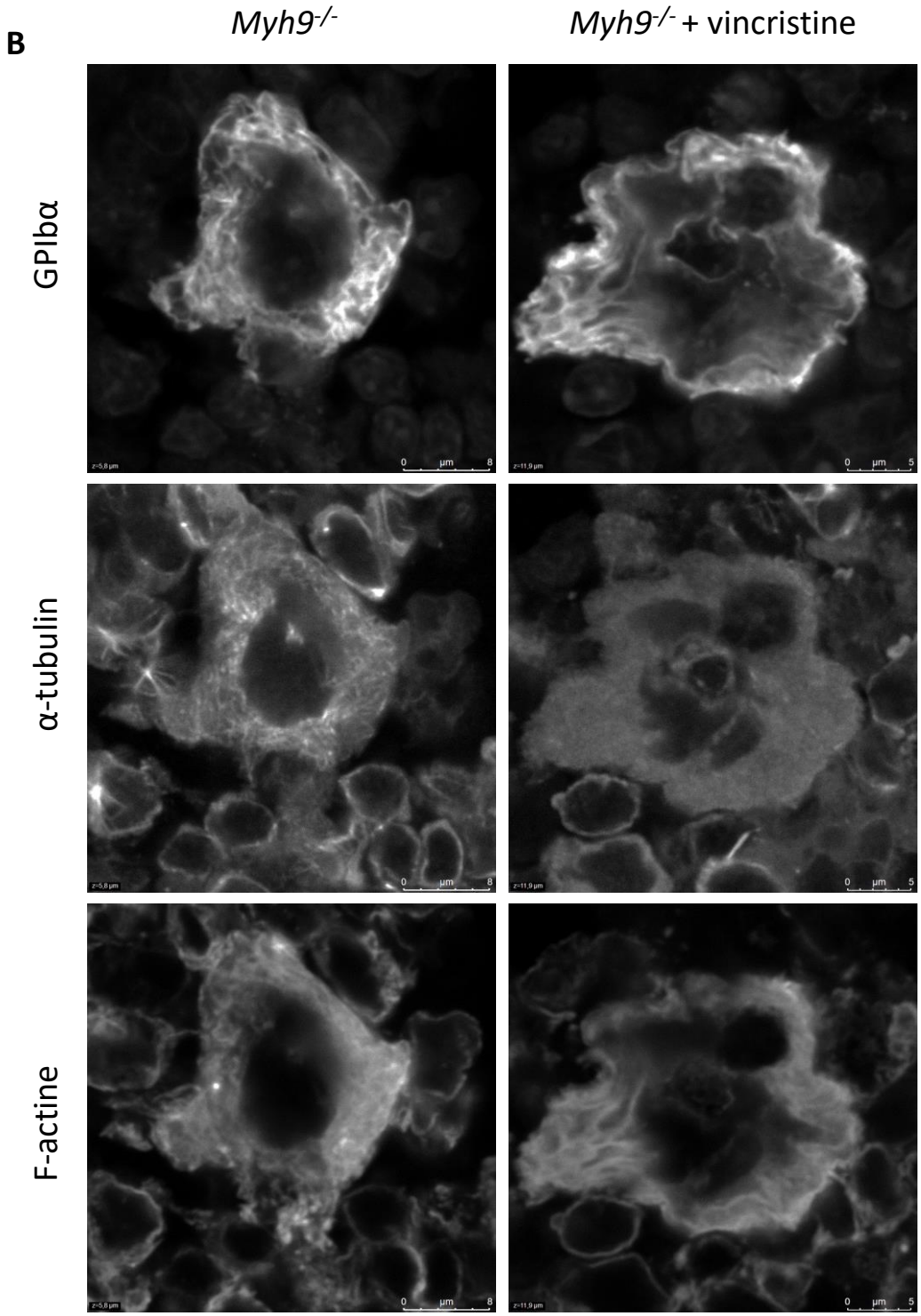

Supplemental Figure S6. Impact of vincristine 1mg/kg injection on nPPT length.

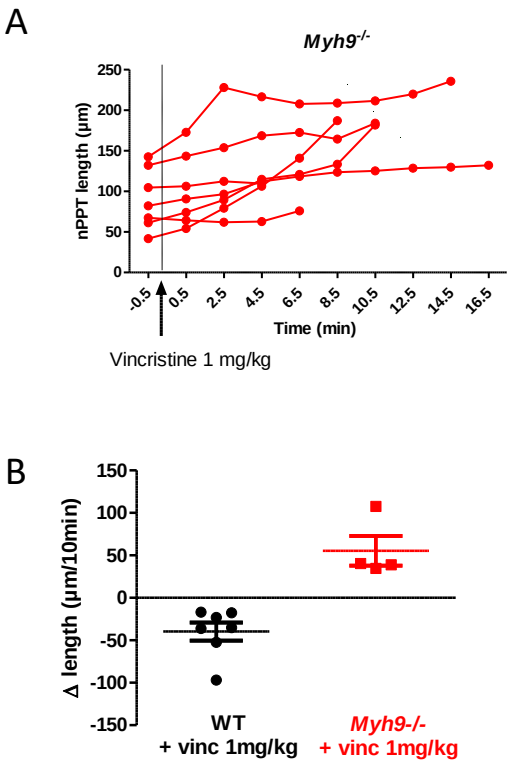

Supplemental Figure S7. *In situ* observation of nPPT from *Myh9*$^{-/-}$ marrow.

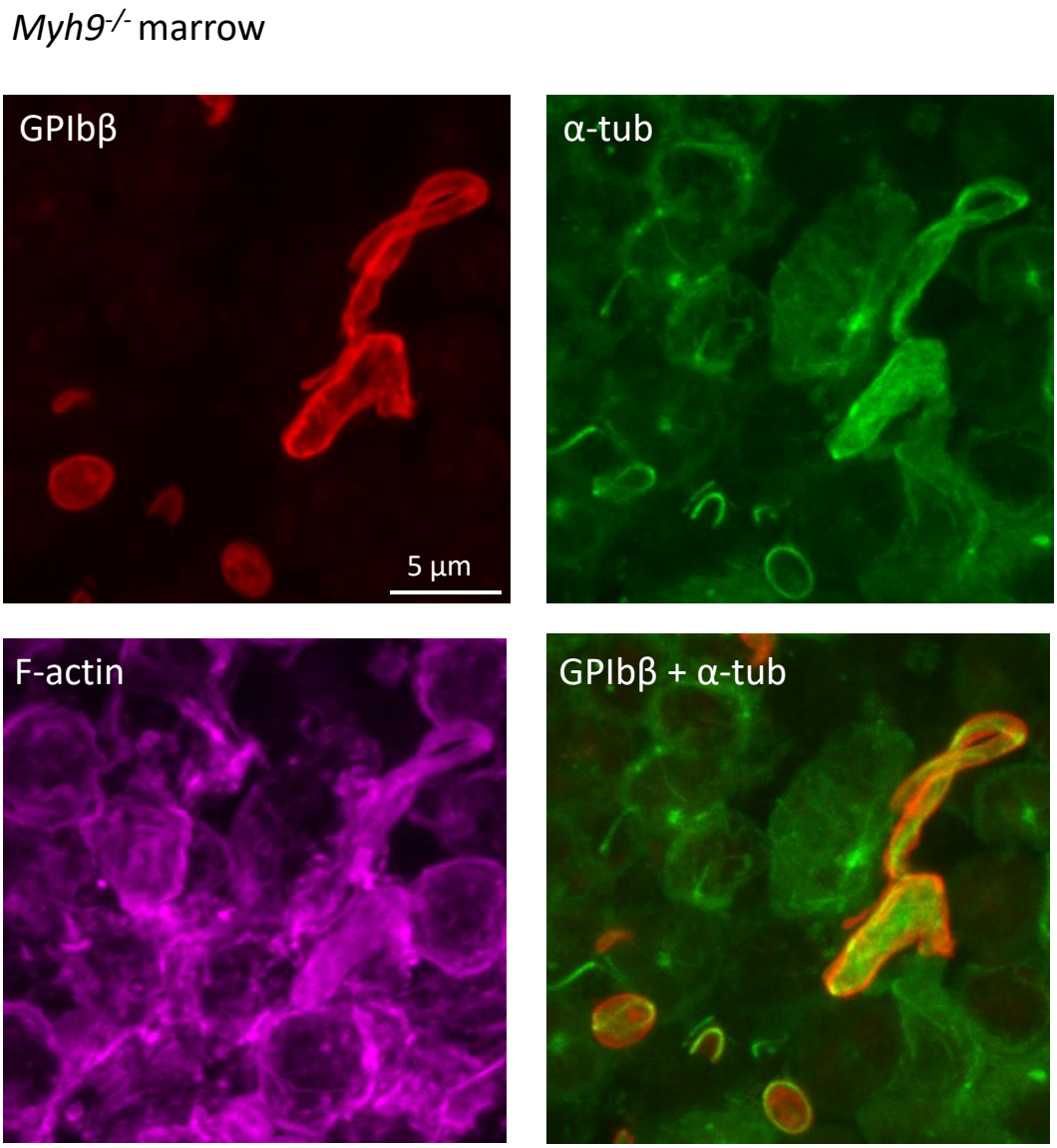

Supplemental Figure S8. *Myh9*$^{-/-}$ nPPT are poorly enriched in DMS.